Journal of Colloid and Interface Science 406 (2013) 44–50

Contents lists available at SciVerse ScienceDirect

Journal of Colloid and Interface Science

www.elsevier.com/locate/jcis

Colloid mobilization by fluid displacement fronts in channels

Volha Lazouskaya [a], Lian-Ping Wang [b], Dani Or [c], Gang Wang [c], Jeffrey L. Caplan [d], Yan Jin [a,*]

[a] Department of Plant and Soil Sciences, University of Delaware, 152 Townsend Hall, Newark, DE 19716, USA
[b] Department of Mechanical Engineering, University of Delaware, 126 Spencer Lab, Newark, DE 19716, USA
[c] Department of Environmental Systems Science, ETH Zurich, Universitaetstrasse 16, 8092 Zurich, Switzerland
[d] Delaware Biotechnology Institute, University of Delaware, 15 Innovation Way, Newark, DE 19711, USA

ARTICLE INFO

Article history:
Received 24 January 2013
Accepted 31 May 2013
Available online 7 June 2013

Keywords:
Colloid transport
Contact line
Drainage
Imbibition
Contact angle
Thin films

ABSTRACT

Understanding colloid mobilization during transient flow in soil is important for addressing colloid and contaminant transport issues. While theoretical descriptions of colloid detachment exist for saturated systems, corresponding mechanisms of colloid mobilization during drainage and imbibition have not been considered in detail. In this work, theoretical force and torque analyses were performed to examine the interactive effects of adhesion, drag, friction, and surface tension forces on colloid mobilization and to outline conditions corresponding to the mobilization mechanisms such as lifting, sliding, and rolling. Colloid and substrate contact angles were used as variables to determine theoretical criteria for colloid mobilization mechanisms during drainage and imbibition. Experimental mobilization of hydrophilic and hydrophobic microspheres with drainage and imbibition fronts was investigated in hydrophilic and hydrophobic channels using a confocal microscope. Colloid mobilization differed between drainage and imbibition due to different dynamic contact angles and interfacial geometries on the contact line. Experimental results did not fully follow the theoretical criteria in all cases, which was explained with additional factors not included in the theory such as presence of aggregates and trailing films. Theoretical force and torque analyses resulted in similar mobilization predictions and suggested that all mobilization mechanisms contributed to the observed colloid mobilization.

1. Introduction

Understanding mobilization of previously deposited colloids or in situ formed colloids in soil is important for assessing concentration of mobile colloids and colloid-associated transport of contaminants (e.g., [1,2]). Several reviews of colloid mobilization and transport in soil and model systems have been published (e.g., [3–5]). However, understanding of the mechanisms controlling colloid mobilization in unsaturated systems is still limited compared to saturated systems [4–6].

El-Farhan et al. [7] and Saiers et al. [8] were among the first to emphasize the role of air–water interface (AWI) in mobilization of soil colloids during transient events, i.e., drainage and imbibition, in unsaturated porous media. Zhuang et al. [9], Cheng and Saiers [1,10], and Chen et al. [6,11] investigated colloid mobilization in column experiments during both drainage and imbibition, but reported inconsistent results on which event was more efficient in colloid mobilization. Visualization experiments to date involved mostly indirect visualization methods such as enumeration of colloids after the passage of air bubbles or successive drainage and imbibition fronts [12–18], which did not distinguish effects of drainage and imbibition. Recently, Aramrak et al. [19] and Lazouskaya et al. [20] observed colloid mobilization during drainage and imbibition directly with a confocal microscope, but worked with a limited range of colloid and substrate properties.

Several researchers indicated that colloids were mobilized on the contact line (where AWI contacts the solid) [14,20,21] and then were transported with the AWI. Lazouskaya et al. [20] used the term front, which encompassed both AWI and the contact line, and therefore emphasized the importance of both in colloid mobilization.

Theoretical descriptions of particle detachment from substrates in either air or water phases are available in the literature (e.g., [22–25]); "detachment" in these studies is equivalent to "mobilization". An attached particle will detach from the substrate when the external forces exceed the adhesion force (between the particle and the substrate) or applied torques on the particle offset the corresponding resisting torque [24,26,27]. Depending on the directions and magnitudes of the forces and torques acting on the

Abbreviations: AWI, air–water interface; DLVO, Derjaguin–Landau–Verwey–Overbeek theory.

* Corresponding author. Fax: +1 302 831 0605.
E-mail addresses: volha@udel.edu (V. Lazouskaya), lwang@udel.edu (L.-P. Wang), dani.or@env.ethz.ch (D. Or), gang.wang@env.ethz.ch (G. Wang), jcaplan@udel.edu (J.L. Caplan), yjin@udel.edu (Y. Jin).

0021-9797/$ - see front matter © 2013 Elsevier Inc. All rights reserved.
http://dx.doi.org/10.1016/j.jcis.2013.05.078

particle, it can be mobilized via lifting off from the substrate, sliding, or rolling along the substrate. It is important to recognize that mobilization by sliding or rolling may not necessarily lead to colloid separation from the substrate, which corresponds to the different modes (i.e., mobile and immobile) of adhesion as studied in Boks et al. [28]. Previously, rolling has been declared as the most likely mobilization mechanism for particles fully submerged in air or water phases (e.g., [24,25]).

Theoretical conceptualization of colloid mobilization with receding and advancing fronts (corresponding to drainage and imbibition, respectively) was originally developed by Leenaars [29] and Leenaars and O'Brien [30] and has been adopted in later studies (e.g., [12,19,20]). The conceptualization is based on the analysis of major forces acting on a colloid on the contact line including surface tension force, adhesion force, and hydrodynamic drag force. Among the forces, the surface tension force (also known as capillary force) was identified as the dominant force responsible for colloid mobilization with displacement fronts [16,29,31]. While these studies provided thorough investigation of the role of the surface tension force in colloid mobilization, the mechanisms of colloid mobilization in two-phase system (i.e., lifting, sliding, and rolling) and corresponding mobilization conditions have not been considered in detail. Shang et al. [31] considered torque balance and rolling possibility for a partially submerged colloid, but to the best of our knowledge, the role of rolling in colloid mobilization on the contact line during imbibition and drainage has not been previously addressed. Extensive analysis of the surface tension force was performed by Gao et al. [32] and Zevi et al. [33], but was applied to colloid retention on the contact line.

In addition to the forces acting on colloids, colloid mobilization and retention have been previously linked to water films that are ubiquitously present in unsaturated porous media (e.g., [34–36]). The ratio of colloid size to film thickness is the major parameter determining potential retention and mobilization (e.g., [34,36]). In addition to the "static" films, e.g., due to adsorbed water or higher water content [37], there are films associated with dynamic processes such as precursor and trailing films observed for advancing and receding fronts [38], which may play an exclusive role in colloid mobilization.

In this work, we investigated colloid mobilization during drainage and imbibition in rectangular capillary channels. The specific objectives were to (1) develop theoretical criteria of colloid mobilization via lifting, sliding and rolling mechanisms during both drainage and imbibition, and (2) examine these criteria experimentally in channels by employing hydrophilic (contact angle generally <90°) and hydrophobic (contact angle generally >90°) colloids and substrates. Special attention was given to thin film configurations and their potential effects on colloid mobilization.

2. Theoretical considerations

2.1. Forces acting on colloids on the contact line

Fig. 1 provides a conceptual schematic of a colloid attached to hydrophilic and hydrophobic substrates and interacting with imbibition and drainage fronts. Fig. 1 also shows two front positions relative to a colloid in each configuration, corresponding to the two surface tension force maxima (as discussed further). Also shown are the adhesion force (directed toward the substrate), hydrodynamic drag force (directed with the flow), and friction force.

Adhesion force (F_A), the physicochemical interaction force between a colloid and the substrate, is calculated with the extended Derjaguin–Landau–Verwey–Overbeek (DLVO) theory [3,39–41] as a sum of van der Waals (F_{vdW}), electrostatic (F_{el}), hydrophobic

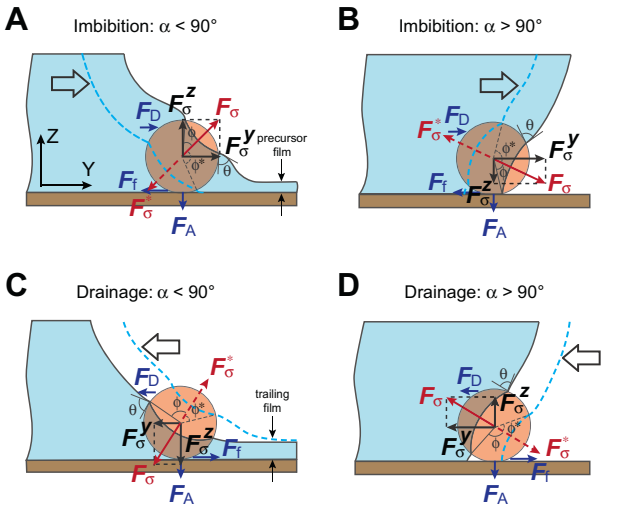

Fig. 1. Colloids interacting with imbibition (A and B) and drainage (C and D) fronts on a hydrophilic and a hydrophobic substrate. Two interface positions on the particle (for the two surface tension force directions, i.e., $\phi > \theta$ and $\phi < \theta$) are shown. The earlier interface position is represented with the dashed line; only surface tension force F_σ^* and position angle ϕ^* are shown for this interface. For the later interface position, the direction and components of surface tension force and other forces are shown. Force arrows do not represent force magnitudes. The large arrows indicate flow direction.

(F_H), and Born repulsion (F_B) forces. Details on each force can be found in the literature [41–44]. Inclusion of Born repulsion in DLVO calculations results in a finite depth of the primary minimum and a more accurate prediction of the force required for colloid mobilization [3,45]. The maximum adhesion force can be found as the maximum attractive (negative) force in the DLVO force profile.

Drag force (F_D) exerted on the attached spherical particle in an imposed shear flow can be calculated as (e.g., [46,47])

$$F_D = \pm 1.701(6\pi\mu G r^2) \quad (1)$$

where the sign depends on whether drainage (−) or imbibition (+) is considered in Fig. 1, μ is fluid viscosity, r is colloid radius, and G is shear rate. The fluid velocity parallel to the substrate is modeled as $v_y = Gz$ where z is the distance from substrate. Because Eq. (1) is derived for a fully submerged stationary particle in a linear shear flow, the drag force on a partially submerged particle will be smaller (e.g., [19]).

Surface tension force (F_σ) acts along the contact between a colloid and AWI and is expressed as

$$F_\sigma = 2\pi r\sigma \sin\phi \sin(\theta - \phi) \quad (2)$$

where σ is the liquid surface tension, θ is the dynamic contact angle on the colloid surface, and ϕ is the angle determining the AWI position on the colloid surface ([29]; Fig. 1). As liquid advances (or recedes) along the particle surface, ϕ changes from 180° to 0° (or 0° to 180°), and surface tension force assumes two magnitude maxima, $F_\sigma = 2\pi r\sigma \sin^2(\theta/2)$ (surface tension force is directed away from the liquid for $\phi < \theta$ and this maximum occurs at $\phi = \theta/2$) and $F_\sigma = -2\pi r\sigma \sin^2(90° + \theta/2)$ (surface tension force is directed toward the liquid for $\phi > \theta$ and this maximum occurs at $\phi = 90° + \theta/2$). For a particle on the contact line, the components of maximum surface tension force (Fig. 1) also depend on the substrate dynamic contact angle, α, and are determined as

$\phi < \theta$:

$$F_\sigma^z = 2\pi r\sigma \sin^2(\theta/2)\cos\alpha \quad (3)$$

$$F_\sigma^y = 2\pi r\sigma \sin^2(\theta/2)\sin\alpha \quad (4)$$

$\phi > \theta$:

$$F_\sigma^z = -2\pi r\sigma \sin^2(90^\circ + \theta/2)\cos\alpha \quad (5)$$

$$F_\sigma^y = -2\pi r\sigma \sin^2(90^\circ + \theta/2)\sin\alpha. \quad (6)$$

In case of imbibition, the particle will first experience the maximum surface tension force according to Eqs. (5) and (6), then, if not mobilized, it will experience the maximum force according to Eqs. (3) and (4). This sequence is reversed for drainage. Also, advancing and receding contact angles instead of the equilibrium contact angle should be used for imbibition and drainage cases, respectively.

Friction force (F_f) acts at the particle contact with the substrate and is proportional to the net normal (downward) force (F_N) holding the particle and substrate together (e.g., [24,27]):

$$F_f = \mu_f F_N \quad (7)$$

where μ_f is the coefficient of static friction, which varies between 0.1 and 2 [24]. For the configuration in Fig. 1, the friction force is determined as

$$F_f = \pm\mu_f F_N = \pm\mu_f(F_\sigma^z + F_A), F_\sigma^z + F_A < 0 \quad (8)$$

where the sign depends on whether drainage (−) or imbibition (+) is considered, and F_A has a negative value.

2.2. Theoretical conditions of colloid mobilization based on force and torque balances

In this work, we define colloid mobilization with drainage or imbibition fronts as colloid displacement from the initial position with the front. Conditions of colloid mobilization via lifting and sliding for partially submerged particles can be determined from the analysis of forces in z- and y-directions (Fig. 1), following the analogy with fully submerged particles (e.g., [24]). The major forces acting in z-direction include adhesion force and the z-component of surface tension force. The net upward force on a particle in z-direction will lead to particle lifting when

$$F_\sigma^z + F_A > 0. \quad (9)$$

In the y-direction, the major forces include drag and friction forces and the y-component of surface tension force. The balance of these forces determines whether the particle will slide in y-direction or remain attached. Sliding occurs when

$$F_\sigma^z + F_A \leqslant 0 \text{ and } |F_\sigma^y + F_D| > |F_f| \quad (10)$$

when neither lifting, nor sliding conditions are satisfied, the particle remains attached, or pinned, to the substrate. Pinning condition can be expressed as

$$F_\sigma^z + F_A \leqslant 0 \text{ and } |F_\sigma^y + F_D| < |F_f| \quad (11)$$

Colloid mobilization due to rolling can occur when a net non-zero torque occurs. Fig. 2 illustrates the torques identified for imbibition and drainage fronts. These include the resisting torque due to adhesion force and applied torques due to drag and surface tension forces. Point O denotes the point of rotation in each configuration, and all torques are calculated with respect to point O [22]. There is no torque due to friction force, which is aligned with point O. Rolling occurs when

$$|F_D l_D| + |F_\sigma l_\sigma| > |F_A l_A|. \quad (12)$$

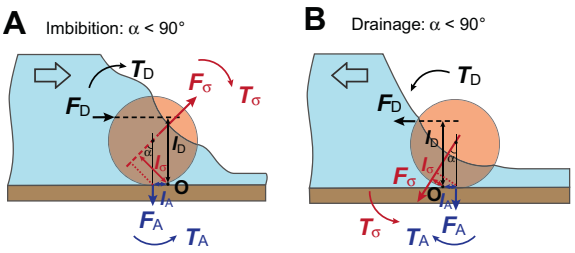

Fig. 2. The forces and torques acting on a particle and shown for imbibition (A) and drainage (B) on a hydrophilic substrate. The corresponding torques are denoted as $T_D = F_D l_D$, $T_A = F_A l_A$, and $T_\sigma = F_\sigma l_\sigma$. The torques are analogous for a hydrophobic substrate and are not shown. The large arrows indicate flow direction.

where l_D, l_σ, and l_A are the lever arms corresponding to drag, surface tension, and adhesion forces, respectively. The lever arm for drag force is calculated as $l_D = 1.37r$ [46,47]. The lever arm for the adhesion force can be determined as the radius of adhesive contact between the particle and the substrate using Johnson–Kendall–Roberts (JKR) theory [22,48]. For particles attached in the primary minima it is found as $l_A = (4F_A r/K)^{1/3}$ where K is the composite Young's modulus ($K = 4.014 \times 10^9$ N m^{-2} for glass and polystyrene contact) [27,49]. Because l_A is small and particle deformation is not known, the lever arm for the surface tension force l_σ can be approximated as $r\sin\alpha$ (the dotted line in Fig. 2). Eq. (12) is approximate and has two important limitations. First, only one of the surface tension force maxima causes the torque, which opposes the resisting torque as shown in Fig. 2. These are $F_\sigma = -2\pi r\sigma \sin^2(90^\circ + \theta/2)$ for drainage ($\phi > \theta$) and $F_\sigma = 2\pi r\sigma \sin^2(\theta/2)$ for imbibition ($\phi < \theta$), except for $\alpha \sim 0^\circ$ during drainage and $\alpha \sim 180^\circ$ during imbibition for which the other two maxima are effective (due to the finite l_A length). Second, l_A represents the adhesive contact due to the DLVO forces only and does not account for the additional load due to normal surface tension force component.

2.3. Thin film configurations

Thin liquid films, i.e., precursor and trailing films, form on hydrophilic surfaces when liquid is receding or advancing, corresponding to drainage and imbibition, respectively.

Precursor films exist ahead of an advancing contact line only when dynamic contact angle is small and the film spreading velocity exceeds the velocity of the contact line [50,51]. Precursor films form and move under the action of attractive van der Waals forces [52]. There are several simplified expressions in the literature that can be used to estimate precursor film thickness (e.g., [50,52,53]). Precursor films are thin, and reported film thickness values range from a few nm [53] up to 100 nm [51].

Trailing (or entrained) films are left on the substrate after the passage of receding contact lines. Film thickness generally depends on the contact line velocity, which is commonly expressed in terms of capillary numbers, $\mathrm{Ca} = \mu v_y/\sigma$ [50,54]. Trailing film thickness (h) is calculated as [55,56]:

$$h = 1.34R\mathrm{Ca}^{2/3} \quad (13)$$

where R is the radius of a capillary or half the distance between two parallel plates. This expression is applicable to capillary numbers between 5×10^{-3} and 10^{-5}; correction for larger Ca can be found in the literature (e.g., [54]). At $\mathrm{Ca} < 10^{-5}$, the experimentally measured films are thicker than predicted by Eq. (13) and no longer depend on Ca [57]. At such low velocity, film becomes very thin and is affected by surface forces [57]. Its thickness can be found from the balance of capillary and van der Waals forces as [54]

$$h = (-AR/6\pi\sigma)^{1/3} \quad (14)$$

where A is the Hamaker constant for the three phases across the film. On a hydrophilic substrate, a stable film will be left behind while on a hydrophobic substrate the film will thin quickly and rupture due to hydrophobic forces (e.g., [58]). On rough surfaces, contact line motion becomes unsteady (e.g., [57]), which additionally affects film thickness.

3. Materials and methods

Two fluorescent colloids were used: yellow-green carboxylate-modified and red sulfate microspheres (F8823 and F8851, Molecular Probes/Invitrogen, Eugene, OR). Both colloids had diameters of 1 μm (1×10^{-6} m) and were suspended in the background solution to final concentrations of 2 ppm (mg L^{-1}), or 3.6×10^6 particles mL^{-1}, of each colloid. Background solutions were prepared by dissolving sodium chloride in deionized water to ionic strengths of 0.01 mol L^{-1} or 0.10 mol L^{-1} and had pH ~ 5.6. Equilibrium contact angles were measured as 29.8 ± 5.0° and 89.5 ± 0.5° for carboxylate-modified and sulfate colloids, which will be referred to as hydrophilic and hydrophobic colloids, respectively. Colloid zeta potentials were measured with Zetasizer Nano ZS (Malvern Instruments, Westborough, MA) for carboxylate-modified (yellow-green) and sulfate (red) colloids as −42.9 ± 1.6 and −24.8 ± 2.1 mV at 0.01 mol L^{-1} and as −33.1 ± 2.8 and −15.4 ± 1.1 mV at 0.10 mol L^{-1} with $n \geqslant 6$ where n is the number of measurements. These values were determined using Smoluchowski approximation.

Channels were the commercially available μ-Slides VI$^{0.4}$ (ibidi®, Martinsried, Germany) with length, width, and height of 17.0 mm, 3.8 mm, and 0.4 mm, respectively. We used hydrophobic (uncoated) and hydrophilic (ibiTreat) channels. Equilibrium and dynamic contact angles of the channels were estimated by imaging water meniscus on the channel wall with a confocal microscope (using a 10× lens). The equilibrium contact angles were determined as 95 ± 3° and 39 ± 5° for hydrophobic and hydrophilic channels, respectively. The values for dynamic contact angles were determined at the flow rate of 0.04 mL h^{-1} and are provided in Table 1. Both channels were negatively charged. Although zeta potentials of the channels could not be measured, the estimate obtained from the manufacturer for similar conditions allowed an assumption of −30 mV for both channels (at the ionic strengths of 0.01 mol L^{-1} for hydrophobic and 0.10 mol L^{-1} for hydrophilic channels).

We performed imbibition and drainage experiments in hydrophobic and hydrophilic channels with suspensions that contained the two types of colloids simultaneously (see a summary in Table 1). Prior to displacement experiments (Fig. 3), colloids were deposited on the substrate (channel surface) in a systematic manner. For hydrophobic channels, colloid suspension with the ionic strength of 0.01 mol L^{-1} was pumped through the channel for 3 h at the flow rate 1 mL h^{-1}; then, the suspension was switched to background solution, which was flushed for 1 h to remove unattached colloids. The same procedure was performed for hydrophilic channels, but at a higher ionic strength (0.10 mol L^{-1}). Because hydrophilic ibidi channels had more negative surfaces than hydrophobic ones, they were used at higher ionic strength to achieve sufficient colloid coverage. Drainage experiment was then continued by allowing air entry into the system and by observing the front at the flow rate of 0.04 mL h^{-1}. Additional step was performed prior to imbibition experiment: after 1 h of flushing with background solution the channel was disconnected from the outlets and was left to evaporate for 2 days. During each imbibition experiment, background solution was introduced into the channel at the flow rate of 0.04 mL h^{-1}.

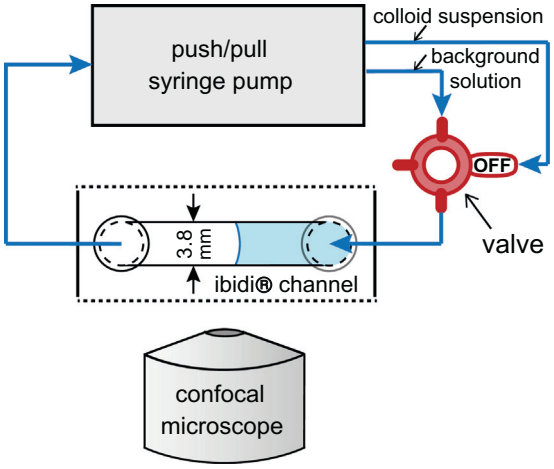

Fig. 3. Key elements of experimental setup.

During displacement experiments, the channels were visualized with a confocal microscope (Zeiss 5 LIVE DUO, Carl Zeiss, Inc., Jena, Germany) using a 25× water-immersion lens (LD LCI Plan-Apochromat 25×, NA 0.8). For imaging both colloid types simultaneously, two lasers were used: Argon/2 (488 nm, for imaging green channel) and DPSS 561-10 (561 nm, for imaging red channel). To observe the contact line, the imaging was performed in the channel mode, i.e., a transmission channel was used along with the green and red channels. Imaging rate was 0.4 frames s^{-1}, and images were acquired with the resolution of 800 × 800 pixels and pixel size of 0.45 μm. The images were further processed with advanced imaging software Volocity 5.4 (PerkinElmer Inc., Waltham, MA) to obtain the numbers of colloids attached to the substrate before and after front passage. Behavior of the two colloids

Table 1
Measured and calculated characteristics of colloid mobilization in channels.

Experimental conditions		Dynamic contact angle, α ($n \geqslant 5$), °	% Hydrophilic colloids mobilized, $n \geqslant 3$ (image pairs)	% Hydrophobic colloids mobilized, $n \geqslant 3$ (image pairs)	Surface tension force components calculated for hydrophilic colloids, N		Surface tension force components calculated for hydrophobic colloids, N	
					z, Eqs. (3) and (5)	y, Eqs. (4) and (6)	z, Eqs. (3) and (5)	y, Eqs. (4) and (6)
Hydrophobic channel	Imbibition	108.6 ± 1.6	Displacement and redeposition	Displacement and redeposition	-4.77×10^{-9} 6.74×10^{-8}	1.42×10^{-8} -2.00×10^{-7}	-3.57×10^{-8} 3.64×10^{-8}	1.06×10^{-7} -1.08×10^{-7}
	Drainage	82.7 ± 5.4	87.9 ± 5.3	84.5 ± 8.7	1.89×10^{-9} -2.68×10^{-8}	1.48×10^{-8} -2.09×10^{-7}	1.42×10^{-8} -1.45×10^{-8}	1.11×10^{-7} -1.13×10^{-7}
Hydrophilic channel	Imbibition	69.7 ± 1.1	99.7 ± 0.5	98.7 ± 1.4	5.18×10^{-9} -7.32×10^{-8}	1.40×10^{-8} -1.98×10^{-7}	3.88×10^{-8} -3.95×10^{-8}	1.05×10^{-7} -1.07×10^{-7}
	Drainage	6.9 ± 0.2	Up to 6.3[a]	Up to 7.7[a]	1.48×10^{-8} -2.10×10^{-7}	1.78×10^{-9} -2.52×10^{-8}	1.11×10^{-7} -1.13×10^{-7}	1.34×10^{-8} -1.36×10^{-8}

[a] The % colloids mobilized under these conditions is close to 0; here, we report the highest colloid removal observed in the experiments.

was investigated under identical experimental conditions by analyzing the two fluorescent channels separately from the same image.

4. Results and discussion

4.1. Mobilization criteria based on colloid and substrate dynamic contact angles

Surface tension force maxima (Eqs. (3)–(6)) depend on colloid radius, surface tension, and colloid and substrate dynamic contact angles. Because the analyzed forces (except for the drag force) are proportional to colloid size, at low flow rate the force analysis is not sensitive to changing colloid size (for particles with $r < 10$ μm). Substantial changes in surface tension are not common. Therefore, colloid and substrate contact angles are the most important parameters affecting colloid mobilization by displacement fronts hence form the criteria for colloid mobilization in this work.

To establish criteria for colloid mobilization via lifting and sliding mechanisms, we first calculated adhesion forces for both hydrophilic and hydrophobic colloids interacting with hydrophilic and hydrophobic channel surfaces using the extended DLVO theory. The hydrophobic forces calculated following the approach of Yoon and Mao [41] and Lazouskaya and Jin [59] were not found substantial in all cases. For estimation of van der Waals and Born repulsion forces, we used the Hamaker constant corresponding to polystyrene–water–quartz system at 1×10^{-20} J (e.g., [60]). The calculated DLVO energy profiles had a finite primary minimum, an energy barrier, and a secondary minimum at all conditions. The corresponding forces necessary to detach colloids from the DLVO primary and secondary minima were found from the force profiles and were on the order of 10^{-9} N and 10^{-14}–10^{-12} N, respectively. The maximum adhesion force was -4.2×10^{-9} N. Drag force, determined with Eq. (1), was on the order of 10^{-13} N (at the velocity of 1×10^{-5} m s^{-1}) and was omitted in further calculations due to its relative insignificance compared to other forces involved. The value $\mu_f = 1$ was used in the friction force calculations.

The values of z- and y-components of the maximum surface tension forces, calculated with Eqs. (3)–(6) for the whole range of colloid and substrate contact angles (0–180°) were used to determine colloid mobilization mechanisms following Eqs. (9)–(11). Mobilizations criteria, i.e., colloid and substrate dynamic contact angles corresponding to each mobilization mechanism, are presented in Fig. 4 (for both surface tension force maxima).

The two diagrams combined show that the majority of possible contact angle combinations lead to colloid mobilization, except for the left bottom corner ($\alpha \sim 0$–$45°$ and $\theta \sim 0$–$15°$) and the right top corner ($\alpha \sim 135$–$180°$ and $\theta \sim 165$–$180°$). For many contact angle combinations in Fig. 4, colloids can be potentially mobilized with both surface tension force maxima (for example, for $\alpha = 70°$ and $\theta = 60°$).

Fig. 4 contains two important features. First, the region for the *sliding* mechanism to operate lies between *no-mobilization* and *lifting*, implying that, for a given colloid contact angle θ, there exists a range of substrate contact angle α where a previously attached colloid becomes mobile tangentially to the substrate due to a front movement. This colloid may stop sliding (thus remain attached to the substrate) or be lifted off, depending on the conditions of the local surface that the colloid enters.

The second feature concerns the likely scenario of colloid mobilization during imbibition and drainage. During imbibition, the condition of $\phi > \theta$ (Fig. 4B) occurs before that of $\phi < \theta$ (Fig. 4A). Therefore, Fig. 4 would imply that for a hydrophobic substrate, during imbibition lifting could take place before sliding while during drainage sliding may occur first, followed by lifting. Similar observations can be made concerning a hydrophilic substrate.

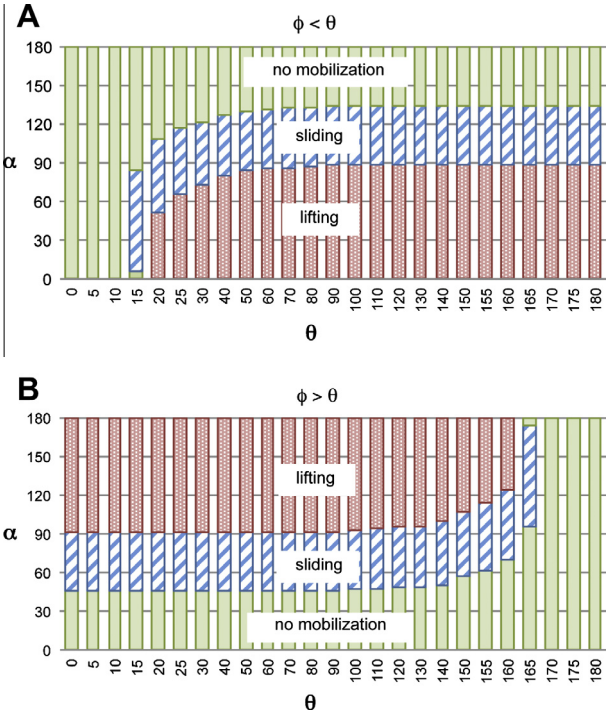

Fig. 4. Mechanisms and criteria (substrate and colloid dynamic contact angles, α and θ) of colloid mobilization based on the two surface tension force maxima (A and B). The values were obtained from calculations with Eqs. (9)–(11) (for 1-μm colloids, water surface tension, the whole range of α and θ, 0–180°, and the maximum adhesion force, -4.2×10^{-9} N).

Although the results in Fig. 4 were obtained relative to a specific adhesion force, they can be extended to other physicochemical conditions. We examined potential effects of substrate and colloid zeta potentials and Hamaker constant on the maximum adhesion force. Zeta potential in the range from −10 to −80 mV typical for quartz [61] did not affect the maximum adhesion force considerably: it changed within the same order of magnitude. The depth of primary minimum increases with Hamaker constant indicating a stronger adhesion force in Eqs. (9)–(11). Such changes could modify the contact angle boundaries by several degrees in the left bottom and right top corners in Fig. 4 but the general trend would remain the same. In general, calculation of the adhesion forces is recommended prior to application of the mobilization criteria in Fig. 4 for conditions other than discussed in this work. Other parameters, which can modify results in Fig. 4, are friction coefficient and front velocity. Smaller μ_f will increase the ranges of substrate contact angles for sliding (Eq. (10)), hence the variation of μ_f needs to be taken into consideration. Drag force can no longer be omitted if the front velocity is several orders of magnitude larger than the values considered in this study.

In addition to lifting and sliding, criteria for colloid rolling were determined with Eq. (12). Calculations show that the applied torque due to surface tension force is large and dominates the resisting torque for most values of θ and α except for the following cases: for imbibition when $\alpha < 5°$ and $\theta = 0$–$20°$ and when $5° < \alpha < 175°$ and $\theta = 0$–$6°$; and for drainage when $\alpha > 175°$ and $\theta = 160$–$180°$ and when $5° < \alpha < 175°$ and $\theta = 174$–$180°$. The values $\alpha = 0°$ and 180°, $\alpha > 175°$ (imbibition), and $\alpha < 5°$ (drainage) were excluded from the torque analysis due to uncertainties associated with l_A and l_σ. Although mobilization criteria found with force and torque analyses overlap for most values of α and θ, there are some combinations of α and θ, for which mobilization is expected either via

lifting/sliding or rolling (e.g., rolling is predicted for $\alpha = 5–45°$ and $\theta = 6–14°$ during imbibition). Therefore, combined force and torque analyses provide a more complete prediction of colloid mobilization. These results also suggest that concurrent lifting/sliding and rolling for the same α and θ values cannot be excluded.

4.2. Experimental examination of the role of colloid and substrate dynamic contact angles in colloid mobilization

Fig. 5 presents confocal images of the two types of colloids interacting with imbibition and drainage fronts in hydrophobic and hydrophilic channels. Quantitative information about colloids mobilized under the four conditions is provided in Table 1.

There was no difference in mobilization of hydrophobic and hydrophilic colloids as reflected in the percentages of mobilized colloids in Table 1. This is in agreement with our mobilization criteria (Fig. 4): both colloids have contact angles in the range where they are subjected to similar mobilization mechanisms. This is in general agreement with the results of Sharma et al. [18]: while they observed slightly more mobilization of sulfate than carboxylate-modified colloids their contact angles differed from the ones reported in this work. Although we used the equilibrium contact angles measured for colloids in Eqs. (3)–(6), the corresponding dynamic contact angles are expected to fall within the approximate range $10° < \theta < 170°$, in which mobilization is effective. These results clearly show that, for both colloid contact angles, lifting and sliding are determined by the substrate contact angle (Fig. 4).

On the hydrophobic substrate, imbibition (Fig. 5B) did not result in considerable mobilization of colloids. Instead, some colloids were displaced along the substrate (typically by 10–50 μm) and redeposited. However, drainage (Fig. 5D) resulted in efficient mobilization of colloids, removing more than 80% colloids. The opposite was observed for the hydrophilic substrate (Fig. 5A and C) where negligible colloid mobilization occurred during drainage while imbibition resulted in almost complete (>95%) mobilization. Aramrak et al. [19] also reported more mobilization of hydrophilic colloids from the hydrophilic substrate with imbibition (80–88%) than drainage (5–10%). Thus, colloid mobilization in channels varied not only between hydrophilic and hydrophobic substrates, but also between imbibition and drainage.

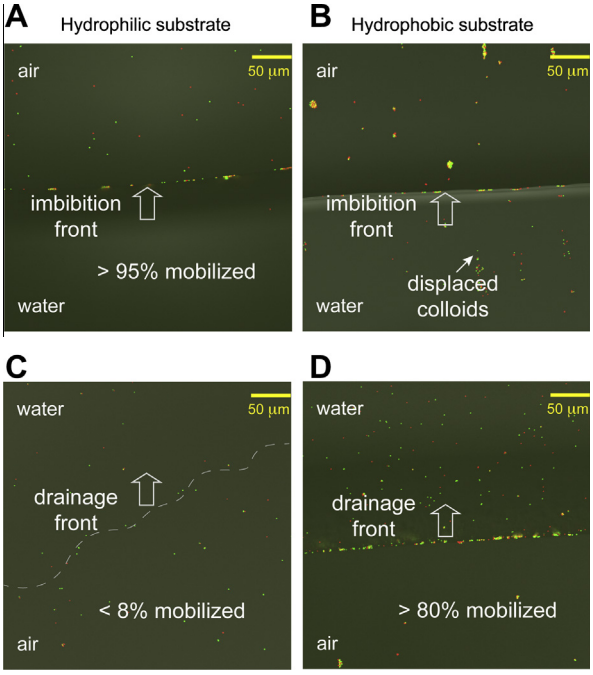

Fig. 5. Confocal images of colloids and imbibition and drainage fronts on hydrophilic (A and C) and hydrophobic (B and D) substrates. The top and bottom parts of each image represent conditions "before" and "after" front passage, respectively. The large arrows indicate the direction of front movement shown for the water phase. Note: Apparent yellow color in the images is due to overlapping of red and yellow-green colloids. When the two channels are viewed separately, no yellow color is observed. (For interpretation of the references to color in this figure legend, the reader is referred to the web version of this article.)

Colloid mobilization was in agreement with the force and torque analyses for the cases in Fig. 5A and D, but not in Fig. 5B and C. The force analysis predicts one or two effective colloid mobilization mechanisms (sliding and/or lifting) to take place in all four cases in Fig. 5. Similarly, the torque analysis (Eq. (11), Fig. 2) predicts rolling to occur for all four cases. Potential explanations on why mobilization was not observed for the cases in Fig. 5B and C include formation of aggregates and presence of thin films on the substrate as discussed further.

For imbibition on hydrophobic substrate ($\alpha = 108°$, Fig. 5B), instead of being completely mobilized as predicted by the theory (Fig. 4), colloids were "displaced" and redeposited (Fig. 5B, bottom). This is likely due to particle aggregation on the hydrophobic substrate. During channel preparation prior to imbibition, evaporating receding contact lines pulled colloids into aggregates on the hydrophobic substrate (Fig. 5B, top) whereas on the hydrophilic substrate the contact lines did not affect colloid distribution resulting in uniform coverage of single particles (Fig. 5A, top). Less efficient mobilization of aggregates compared to single particles was reported by Leenaars [29] and Leenaars and O'Brien [30], due to different relative importance of forces for particles (or aggregates) with $r > 10$ μm [8,13,29,62].

Presence of thin films on the substrate is critical for colloid mobilization because it can modify the surface tension force treatment (e.g., by changing front position on the particle and preventing certain surface tension force configurations for a given substrate contact angle) and, depending on film thickness, can result in film straining of colloids. The potential effects of thin films could explain the limited mobilization observed in Fig. 5C and will be considered in the next section.

4.3. Potential effects of film thickness

Among interfacial geometries in Fig. 1, stable films potentially exist only on the hydrophilic substrate. Although our microscopic observations cannot resolve film thickness, it can be estimated theoretically. Advancing contact angle in hydrophilic channels is relatively large ($\alpha = 69.7°$), and therefore no precursor film is expected in Fig. 5A. For the small capillary number in our experiments ($Ca = 1.2 \times 10^{-7}$), trailing film thickness in Fig. 5C was estimated with Eq. (14) as ~11.4 nm, with Hamaker constant for air–water–quartz system equal to -1.0×10^{-20} J [63] and with the channel half-width of 0.2 mm as parameter R. Because the predicted trailing film is thin, negligible colloid mobilization during drainage in hydrophilic channels (Fig. 5C) was likely caused by colloid pinning within the extended meniscus at small receding contact angle ($\alpha = 6.9°$) and not within the trailing film. This film configuration is similar to film straining [34], which involved retention of hydrophilic colloids within disconnected films (equivalent to $\alpha \sim 0°$).

Trailing films thicker than predicted by Eq. (14) could occur due to unsteady front motion. On rough surfaces, the contact line motion is unsteady [57] and accompanied with contact line jumps. The velocity of interfacial jumps can substantially exceed the mean front velocity [64] and thus result in thicker trailing films (Eq. (13)). In this work, however, the channel surfaces were smooth per manufacturer's specification. Apart from pinning within the film, no mobilization will take place for the films larger than

colloid size due to lack of particle-front interception. Contact lines in natural porous media, having hydrophilic and rough surfaces, will move with interfacial jumps, and thus thicker trailing films are expected than the ones calculated with Eq. (14) or based on mean front velocity (Eq. (13)). Therefore, during drainage in natural porous media trailing film thickness can modify interfacial geometry (e.g., front position on the particle) and make the proposed theoretical analysis inaccurate.

5. Conclusions

Through analysis of force and torque balances for colloids on the contact line, we provided theoretically determined criteria for colloid mobilization by different mechanisms, i.e., lifting, sliding, and rolling. Previously, rolling as a mechanism of colloid mobilization on the contact line has not been considered, therefore, this work represents a more complete treatment of colloid mobilization during drainage and imbibition. Our analysis indicates that colloids could experience both translational and rotational motion and be mobilized via all three mechanisms, which are largely determined by substrate dynamic contact angle.

Experimental results, however, did not fully agree with theoretical predictions. The theory overestimates colloid mobilization in the cases where additional parameters such as colloid aggregates and trailing films, not included in the idealized analysis, affect mobilization. These factors need to be considered prior to application of the presented theoretical analysis.

The theoretical analysis and experimental observations suggest that imbibition and drainage fronts mobilize colloids differently because of the intrinsic differences (e.g., dynamic contact angles, presence of films, and effective torques) between the two fronts. Therefore, literature results on colloid mobilization by imbibition and drainage in porous media should not be compared directly without considering their differences. In addition, contact angles are often not reported in the published studies for the investigated model or natural systems, making comparison between different studies more difficult. This work suggests that contact angle estimates for the systems of interest would be very useful for an initial colloid mobilization assessment.

The theoretical framework presented here is a comprehensive description of the interface-scale colloid mobilization mechanisms and can be utilized for conditions beyond the ones examined in this study. It should be noted that additional factors would need to be considered at larger scales to predict effective mobilization and transport in porous media. In addition to the model systems investigated in this work, accurate theoretical prediction of colloid mobilization with displacement fronts in soil will benefit from work with more realistic systems, including irregular and rough colloids and substrates.

Acknowledgments

This study was supported by United States Department of Agriculture (USDA)-National Research Initiative (NRI) Competitive Grant No. 2008-00653, by National Science Foundation (NSF) CBET-0932686, and by German Research Foundation (DFG-FOR 1083) on Multi-Scale Interfaces in Unsaturated Soil (MUSIS). The authors are grateful to Dr. Yuniati Zevi, Wenjuan Zheng and Dr. Chao Wang of the University of Delaware and to Franziska Moebius and Daniel Breitenstein of ETH-Zurich for the assistance with experiments and fruitful discussions.

References

[1] T. Cheng, J.E. Saiers, Water Resour. Res. 45 (2009) W08414.
[2] E. Michel, S. Majdalani, L. Di-Pietro, Vadose Zone J. 9 (2010) 307.
[3] J.N. Ryan, M. Elimelech, Colloids Surf. A 107 (1996) 1.
[4] N.M. DeNovio, J.E. Saiers, J.N. Ryan, Vadose Zone J. 3 (2004) 338.
[5] T.K. Sen, K.C. Khilar, Adv. Colloid Interface Sci. 119 (2006) 71.
[6] L. Chen, D.A. Sabatini, T.C.G. Kibbey, Environ. Sci. Technol. 42 (2008) 1916.
[7] Y.H. El-Farhan, N.M. DeNovio, J.S. Herman, G.M. Hornberger, Environ. Sci. Technol. 34 (2000) 3555.
[8] J.E. Saiers, G.M. Hornberger, D.B. Gower, J.S. Herman, Geophys. Res. Lett. 30 (2003) 2083.
[9] J. Zhuang, J.F. McCarthy, J.S. Tyner, E. Perfect, M. Flury, Environ. Sci. Technol. 41 (2007) 3199.
[10] T. Cheng, J.E. Saiers, Environ. Sci. Technol. 44 (2010) 7443.
[11] L. Chen, D.A. Sabatini, T.C.G. Kibbey, J. Contam. Hydrol. 118 (2010) 199.
[12] J. Noordmans, P.J. Wit, H.C. van der Mei, H.J. Busscher, J. Adhes. Sci. Technol. 11 (1997) 957.
[13] C. Gómez Suarez, J. Noordmans, H.C. van der Mei, H.J. Busscher, Langmuir 15 (1999) 5123.
[14] C. Gómez Suárez, J. Noordmans, H.C. van der Mei, H.J. Busscher, Phys. Chem. Chem. Phys. 1 (1999) 4423.
[15] C. Gómez-Suárez, H.C. van der Mei, H.J. Busscher, Colloids Surf. A 186 (2001) 211.
[16] C. Gómez-Suárez, H.J. Busscher, H.C. van der Mei, Appl. Environ. Microbiol. 67 (2001) 2531.
[17] B. Gao, J.E. Saiers, J. Ryan, Water Resour. Res. 42 (2006) W01410.
[18] P. Sharma, M. Flury, J. Zhou, J. Colloid Interface Sci. 326 (2008) 143.
[19] S. Aramrak, M. Flury, J.B. Harsh, Langmuir 27 (2011) 9985.
[20] V. Lazouskaya, L.-P. Wang, H. Gao, X. Shi, K. Czymmek, Y. Jin, Vadose Zone J. 10 (2011) 1250.
[21] M.R. Parini, D.L. Eggett, W.G. Pitt, J. Clin. Periodontol. 32 (2005) 1151.
[22] H.-C. Wang, Aerosol Sci. Technol. 13 (1990) 386.
[23] C.-J. Tsai, D.Y.H. Pui, B.Y.H. Liu, J. Aerosol Sci. 22 (1991) 737.
[24] J. Bergendahl, D. Grasso, Colloids Surf. A 135 (1998) 193.
[25] G. Ahmadi, S. Guo, X. Zhang, Particul. Sci. Technol. 25 (2007) 59.
[26] S. Torkzaban, S.A. Bradford, S.L. Walker, Langmuir 23 (2007) 9652.
[27] S.A. Bradford, S. Torkzaban, A. Wiegmann, Vadose Zone J. 10 (2011) 252.
[28] N.P. Boks, H.J. Kaper, W. Norde, H.C. van der Mei, H.J. Busscher, J. Colloid Interface Sci. 331 (2009) 60.
[29] A.F.M. Leenaars, A new approach to the removal of sub-micron particles from solid (silicon) substrates, in: K.L. Mittal (Ed.), Particles on Surfaces 1: Detection, Adhesion, and Removal, Plenum Press, New York, 1988, pp. 361–372.
[30] A.F.M. Leenaars, S.B.G. O'Brien, Philips J. Res. 44 (1989) 183.
[31] J. Shang, M. Flury, G. Chen, J. Zhuang, Water Resour. Res. 44 (2008) W06411.
[32] B. Gao, T.S. Steenhuis, Y. Zevi, V.L. Morales, J.L. Nieber, B.K. Richards, J.F. McCarthy, J.-Y. Parlange, Water Resour. Res. 44 (2008) W04504.
[33] Y. Zevi, B. Gao, W. Zhang, V.L. Morales, M.E. Cakmak, E.A. Medrano, W. Sang, T.S. Steenhuis, Water Res. 46 (2012) 295.
[34] J. Wan, T.K. Tokunaga, Environ. Sci. Technol. 31 (1997) 2413.
[35] S. Veerapaneni, J. Wan, T.K. Tokunaga, Environ. Sci. Technol. 34 (2000) 2465.
[36] J. Shang, M. Flury, Y. Deng, Water Resour. Res. 45 (2009) W06420.
[37] T.K. Tokunaga, Water Resour. Res. 45 (2009) W06415.
[38] G.J. Hirasaki, S.Y. Yang, Dynamic contact line with disjoining pressure, large capillary numbers, large angles and pre-wetted, precursor, or entrained films, in: K.L. Mittal (Ed.), Contact Angle, Wettability and Adhesion, vol. 2, VSP, Utrecht, 2002, pp. 1–30.
[39] B.V. Derjaguin, L. Landau, Acta Physicochim. URSS 14 (1941) 633.
[40] E.J.W. Verwey, J.Th.G. Overbeek, Theory of the Stability of Lyophobic Colloids, Elsevier, New York, 1948.
[41] R.-H. Yoon, L. Mao, J. Colloid Interface Sci. 181 (1996) 613.
[42] R. Hogg, T.W. Healy, D.W. Fuerstenau, Trans. Faraday Soc. 62 (1966) 1638.
[43] J. Gregory, J. Colloid Interface Sci. 83 (1981) 138.
[44] T. Mahmood, A. Amirtharajah, T.W. Sturm, K.E. Dennett, Colloids Surf. A 177 (2001) 99.
[45] E. Ruckenstein, D.C. Prieve, AIChE J. 22 (1976) 276.
[46] A.J. Goldman, R.G. Cox, H. Brenner, Chem. Eng. Sci. 22 (1967) 653.
[47] M.E. O'Neill, Chem. Eng. Sci. 23 (1968) 1293.
[48] K.L. Johnson, K. Kendall, A.D. Roberts, Proc. Roy. Soc. Lond. A 324 (1971) 301.
[49] J. Bergendahl, D. Grasso, Chem. Eng. Sci. 55 (2000) 1523.
[50] J.F. Joanny, Phys. Scripta T29 (1989) 270.
[51] S.F. Kistler, Hydrodynamics of wetting, in: J.C. Berg (Ed.), Wettability, Surfactant Science Series, vol. 49, Marcel Dekker, New York, 1993, pp. 311–429.
[52] O.V. Voinov, J. Colloid Interface Sci. 188 (1997) 1.
[53] P.G. de Gennes, Rev. Mod. Phys. 57 (1985) 827.
[54] D. Quéré, Annu. Rev. Fluid Mech. 31 (1999) 347.
[55] F.P. Bretherton, J. Fluid Mech. 10 (1961) 166.
[56] M.T. Kreutzer, F. Kapteijn, J.A. Moulijn, J.J. Heiszwolf, Chem. Eng. Sci. 60 (2005) 5895.
[57] G.F. Teletzke, H.T. Davies, L.E. Scriven, Rev. Phys. Appl. 23 (1988) 989.
[58] L. Pan, R.-H. Yoon, Faraday Discuss. 146 (2010) 325.
[59] V. Lazouskaya, Y. Jin, Colloids Surf. A 325 (2008) 141.
[60] N. Tufenkji, M. Elimelech, Langmuir 21 (2005) 841.
[61] S.A. Bradford, S. Torkzaban, Vadose Zone J. 7 (2008) 667.
[62] S.B.G. O'Brien, B.H.A.A. van den Brule, J. Colloid Interface Sci. 144 (1991) 210.
[63] J.N. Israelachvili, Intermolecular and Surface Forces, Academic Press, London, 1991.
[64] F. Moebius, D. Or, J Colloid Interface Sci. 377 (2012) 406.